

Phase Diagram of the Kitaev-type Model on a Decorated Honeycomb Lattice in the Isolated Dimer Limit

Joji Nasu¹ and Yukitoshi Motome²

¹ Tokyo Institute of Technology, Ookayama, Meguro, Tokyo, Japan
nasu@phys.titech.ac.jp

² University of Tokyo, Hongo, Bunkyo, Tokyo, Japan
motome@ap.t.u-tokyo.ac.jp

Abstract

An effective model in the isolated dimer limit of the Kitaev-type model on a decorated honeycomb lattice is investigated at finite temperature. The ground state of this model is exactly shown to be a chiral spin liquid with spontaneous breaking of time reversal symmetry. We elaborate the finite-temperature phase diagram by using the mean-field approximation and Monte Carlo simulation. We find that the phase transition between the high-temperature paramagnetic phase and the low-temperature chiral spin liquid phase is always of second order in the Monte Carlo results, although a tricritical point appears in the mean-field phase diagram. The finite-size scaling analysis of the Monte Carlo data suggests that the phase transition belongs to the two-dimensional Ising universality class.

Keywords: Kitaev model, chiral spin liquid, toric code, Monte Carlo simulation

1 Introduction

A Mott insulator without magnetic ordering down to the lowest temperature (T) has attracted considerable attention in strongly correlated electron systems [1]. This state, called the quantum spin liquid, is brought about by strong quantum fluctuations, which often become conspicuous in low-dimensional systems and in the presence of geometrical frustration of the lattice structures. Several candidates of quantum spin liquids have been found theoretically and experimentally in quantum spin systems on geometrically frustrated lattices. Among them, the chiral spin liquid (CSL), where the time reversal symmetry is broken despite the absence of magnetic order, is of particularly interesting and has been discussed [2–10].

As a simple realization of CSL, a Kitaev-type model defined on a decorated honeycomb lattice has been studied in the last decade [11–17]. This is a variant of the Kitaev model on the honeycomb lattice [11], for which the ground state is exactly shown to be a CSL. The decorated honeycomb lattice is constructed from the honeycomb lattice by replacing the sites by triangles [see Fig. 1(a)]. Interestingly, this model exhibits two types of CSLs, topologically

trivial (with Abelian anyon excitations) and nontrivial (with non-Abelian anyon excitations), by changing the exchange constants [12]. The characteristics of the CSL ground states were also studied for the effective models in two limits, the isolated dimer limit and the isolated triangle limit [13]. Recently, the authors studied the finite- T properties of CSLs for the original Kitaev-type model by using the quantum Monte Carlo (MC) simulation [17]. In addition to the finite- T phase transition associated with the time reversal symmetry breaking, peculiar crossovers were found in the regions near the two limiting cases. Although the results were compared with the asymptotic behaviors expected in the two limits, the details were not reported in the previous study [17]. In order to further understand the mechanism of the crossovers and the phase transition, it is desired to elucidate the finite- T properties of the effective models in these limiting cases.

In this paper, we investigate thermodynamic properties in the isolated dimer limit of the Kitaev-type model on the decorated honeycomb lattice. In this limit, the effective model is described by Ising-type Z_2 variables only. Performing the mean-field (MF) approximation and an unbiased MC simulation, we elaborate the finite- T phase diagram. In both calculations, we find that the system exhibits a phase transition associated with the time reversal symmetry breaking at a finite T . The phase transition is always of second order in the MC simulation, whereas both first- and second-order transitions appear with a tricritical point in the MF approximation. We also find a crossover above the critical temperature, associated with the coherent alignment of local conserved quantities. Moreover, the analysis of the finite-size scaling indicates that the phase transition belongs to the two-dimensional Ising universality class.

2 Model

We begin with a variant of the Kitaev model defined on a decorated honeycomb lattice depicted in Fig. 1(a), whose Hamiltonian is given by [12]

$$\mathcal{H} = - \sum_{\gamma=x,y,z} \sum_{\langle ij \rangle_\gamma} J_\gamma \sigma_i^\gamma \sigma_j^\gamma - \sum_{\gamma=x,y,z} \sum_{\langle ij \rangle'_\gamma} J'_\gamma \sigma_i^\gamma \sigma_j^\gamma, \quad (1)$$

where σ_i^γ is the $\gamma (= x, y, z)$ component of the Pauli matrices, representing an $S = 1/2$ spin located on site i ; $\langle ij \rangle_\gamma$ and $\langle ij \rangle'_\gamma$ stand for the intra- and inter-triangle bonds, respectively [see Fig. 1(a)]. For simplicity, we take $J_x = J_y = J_z = J$ and $J'_x = J'_y = J'_z = J'$, as in Ref. [12].

There are two kinds of conserved quantities in this model: $W_d = \prod_{i \in d} \sigma_i^{\gamma_i}$ and $W_t = \prod_{i \in t} \sigma_i^{\gamma_i}$, where d (t) represents a set of the sites belonging to a dodecagon (triangle) loop on the decorated honeycomb lattice, and γ_i corresponds to the bond component not included in the loop d or t among three bonds connected to the site i . These conserved quantities are Z_2 variables taking the values ± 1 . Note that W_t changes its sign by the time reversal operation, as it consists of the product of three spins. The ground state of this model is a CSL in which the time reversal symmetry is broken by uniform alignment of W_t as well as W_d [12].

In the present study, we are particularly interested in the limit of $J' \gg J$, where the dimers on the inter-triangle bonds are weakly coupled by J . This is called the isolated dimer limit. When each inter-triangle dimer is regarded as a site, the dimers form a kagome lattice, as shown in Fig. 1(b). The effective interaction between the dimers is derived by the perturbation expansion in terms of J/J' [13]. The effective Hamiltonian is written in the form of

$$\mathcal{H}_{\text{eff}} = E_0 - C_h \sum_h \tilde{W}_h - C_t \sum_{\langle ht_1 t_2 \rangle} \tilde{W}_h \tilde{W}_{t_1} \tilde{W}_{t_2}, \quad (2)$$

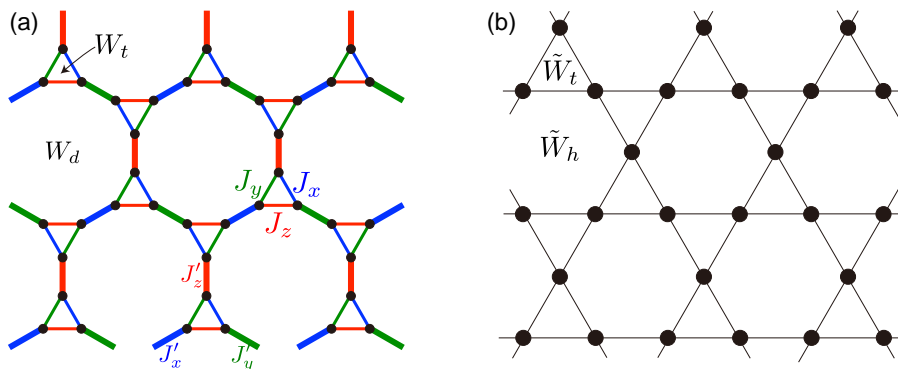


Figure 1: (a) Schematic picture of the model in Eq. (1) on a decorated honeycomb lattice. Thin and thick lines represent the intra- and inter-triangle bonds, respectively. (b) A kagome lattice on which the effective model in Eq. (2) is defined.

where \tilde{W}_h and \tilde{W}_t are conserved quantities given by the projection of W_d and W_t onto the dimer subspace; they are also Z_2 variables taking ± 1 . As shown in Fig. 1(b), \tilde{W}_h and \tilde{W}_t are defined on hexagons and triangles, respectively. Similar to W_t , \tilde{W}_t also changes its sign by the time reversal operation. The coefficients in Eq. (2) are given by $C_h = \frac{63}{256} \frac{J^6}{J'^5} - \frac{297}{1024} \frac{J^8}{J'^7}$ and $C_t = \frac{33}{2048} \frac{J^8}{J'^7}$; E_0 is a constant, and the sum of $\langle ht_1 t_2 \rangle$ is taken over three neighboring plaquettes [13].

In the following calculations, we parameterize the coefficients in Eq. (2) as $C_h = x$ and $C_t = (1-x)/15$ by introducing $x \in [0 : 1]$. The limit of $J' \gg J$ corresponds to $x \rightarrow 1$, where the second term in Eq. (2) is dominant over the third term. In the present study, however, we analyze the effective model in Eq. (2) in the whole region of x , i.e., $0 \leq x \leq 1$, in order to elucidate the thermodynamic properties of this model.

3 Method

We investigate thermodynamic properties of the effective model in Eq. (2) using the MF approximation and the MC simulation. In the MF approximation, the interaction between \tilde{W}_h and \tilde{W}_t in the last term in Eq. (2) is decoupled by introducing the mean fields $\langle \tilde{W}_h \rangle$ and $\langle \tilde{W}_t \rangle$. The resultant MF Hamiltonian per unit cell is given by

$$\mathcal{H}_{\text{eff}}^{\text{MF}} = -(x + (1-x)\langle \tilde{W}_t \rangle^2)W_h - 2(1-x)\langle \tilde{W}_h \rangle \langle \tilde{W}_t \rangle \tilde{W}_t + 2(1-x)\langle \tilde{W}_h \rangle \langle \tilde{W}_t \rangle^2, \quad (3)$$

up to a constant. From this form, the self-consistent equations for the mean fields are given by

$$\langle \tilde{W}_h \rangle = \tanh[\beta\{x + (1-x)\langle \tilde{W}_t \rangle^2\}], \quad (4)$$

$$\langle \tilde{W}_t \rangle = \tanh\{2\beta(1-x)\langle \tilde{W}_h \rangle \langle \tilde{W}_t \rangle\}, \quad (5)$$

where $\beta = 1/T$ is the inverse temperature (we set the Boltzmann constant $k_B = 1$). By solving the above equations and minimizing the free energy, we calculated the thermal averages $\langle \tilde{W}_h \rangle$ and $\langle \tilde{W}_t \rangle$.

In the MC simulation, one can apply a classical MC method as the model in Eq. (2) includes only the Ising type variables \tilde{W}_h and \tilde{W}_t . We adopted the Wang-Landau algorithm [18, 19]:

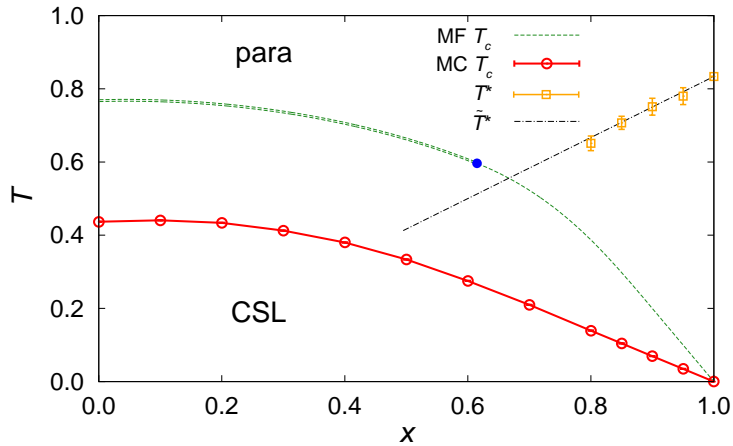


Figure 2: Phase diagram of the effective model in Eq. (2). The horizontal axis x is defined so that $C_h = x$ and $C_t = (1-x)/15$ in Eq. (2). The single- and double-dashed green lines represent the critical temperature T_c for the second- and first-order phase transition obtained by the MF calculation; the blue filled circle represents the tricritical point. The open circles connected by the solid red line and the open squares represent T_c and T^* obtained by the MC simulation, respectively. The dashed-dotted line indicates a crossover temperature \tilde{T}^* estimated for an effective two-level system. See the text for details.

after obtaining the density of states iteratively, we spent 10^6 MC steps for measurement and performed them 10 times, independently. We carried out the simulations for the finite-size clusters including $N = 3L^2$ of \tilde{W}_h and \tilde{W}_t up to $L = 50$ under the periodic boundary conditions.

4 Results

4.1 Mean-field calculation

The phase diagram obtained by the MF calculations is shown in Fig. 2. There is a phase transition between two phases, the high- T paramagnetic phase and the low- T CSL phase, associated with the time reversal symmetry breaking. The phase boundary is calculated as follows. As the CSL phase is characterized by the chiral order parameter $\langle \tilde{W}_t \rangle$, let us consider the expansion of the free energy per unit cell in terms of $\langle \tilde{W}_t \rangle$ as

$$F^{\text{MF}} = -\frac{1}{\beta} \ln \text{Tr} e^{-\beta \mathcal{H}_{\text{eff}}^{\text{MF}}} = f_0 + f_2 \langle \tilde{W}_t \rangle^2 + f_4 \langle \tilde{W}_t \rangle^4 + \dots, \quad (6)$$

where the coefficients are given by

$$f_2 = 2(1-x)\{1 - 2\beta(1-x) \tanh \beta x\} \tanh \beta x, \quad (7)$$

$$f_4 = 4\beta(1-x)^2 [3\{3 - 8\beta(1-x) \tanh \beta x\}(1 - \tanh^2 \beta x) + 8\beta^2(1-x)^2 \tanh^4 \beta x]. \quad (8)$$

When the transition is of second order, the critical temperature T_c is determined by $f_2 = 0$ with $f_4 > 0$, which leads to the equation $1 = 2\beta(1-x) \tanh \beta x$. We find that this condition is

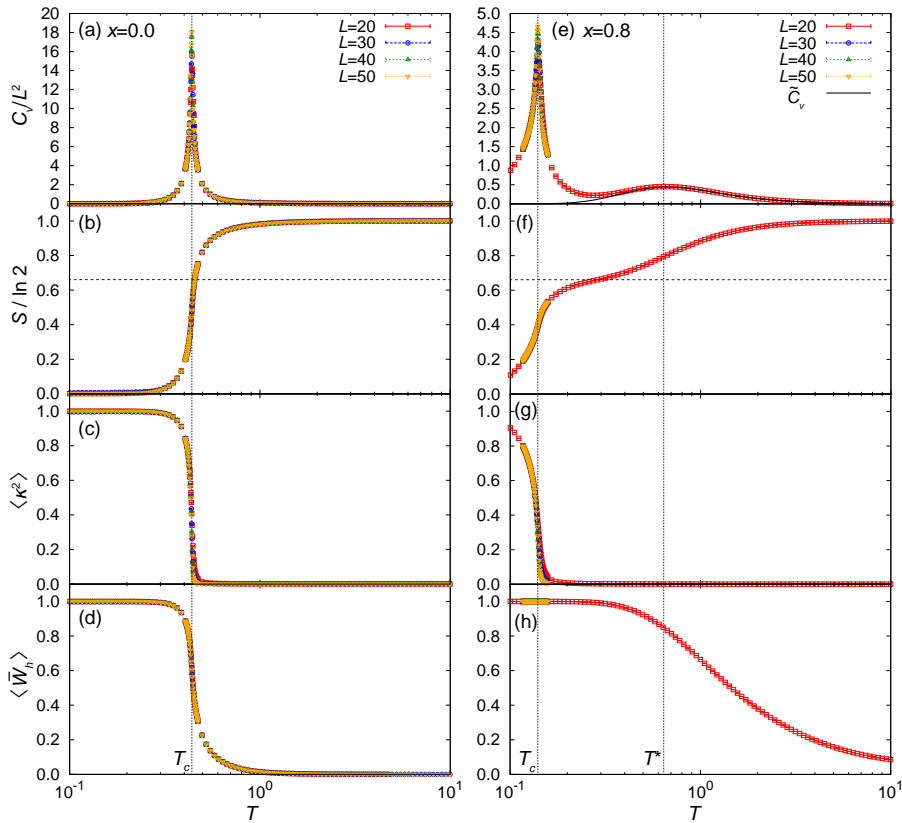


Figure 3: (a) T dependences of (a) the specific heat, (b) the entropy per site, (c) the mean square of the chiral order parameter κ , and (d) the mean of \bar{W}_h per hexagon at $x = 0.0$ obtained by the MC simulation. (e)-(f) Corresponding data at $x = 0.8$. For comparison, the specific heat for an effective two-level model, \bar{C}_v , is also shown in (e). The vertical dotted lines indicate T_c and T^* . The horizontal dotted lines in (b) and (f) represent $S = \frac{2}{3} \ln 2$.

indeed met in the region near $x = 1$; the obtained T_c is shown by the single-dashed green line in Fig. 2. In the vicinity of $x = 1$, T_c arises linearly from zero, as the interaction coefficient C_t in Eq. (2) is proportional to $(1 - x)$. While decreasing x , f_4 decreases to zero, which results in the tricritical point with $f_2 = f_4 = 0$ at $(x_{\text{tri}}, T_{\text{tri}}) \simeq (0.615, 0.596)$, as shown in Fig. 2. For $x < x_{\text{tri}}$, the phase transition becomes first order; in this region, T_c is determined by comparing two local minima of F^{MF} at $\langle \bar{W}_t \rangle = 0$ and $\langle \bar{W}_t \rangle > 0$. The obtained value of T_c for the first-order phase transition is presented by the double-dashed green line in Fig. 2.

4.2 Monte Carlo simulation

We further examined the finite- T properties by the MC simulation, in which the effect of thermal fluctuations is taken into account beyond the MF approximation. Figure 3 shows typical MC results for T dependences of physical quantities. First, we discuss the data at $x = 0$. Figure 3(a) shows the specific heat for several cluster sizes. There is a peak that

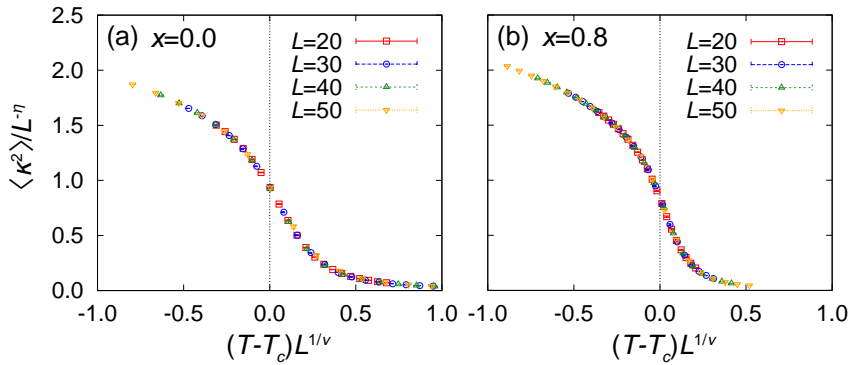


Figure 4: Scaling collapses for $\langle \kappa^2 \rangle$ at (a) $x = 0.0$ with $T_c = 0.4367$, $1/\nu = 1.027$, and $\eta = 0.243$ at $x = 0.0$ and (b) $x = 0.8$ with $T_c = 0.13906$, $1/\nu = 1.001$, and $\eta = 0.2545$.

becomes sharper for larger L . The result indicates that the system exhibits a phase transition at $T_c \simeq 0.44$. Through this transition, all of the entropy $\ln 2$ is released, as shown in Fig. 3(b). Indeed, both \tilde{W}_t and \tilde{W}_h grow coherently at T_c . As shown in Fig. 3(c), the mean square of \tilde{W}_t , $\langle \kappa^2 \rangle$, where $\kappa = \frac{1}{2L^2} \sum_t \tilde{W}_t$, abruptly increases below T_c with decreasing T , indicating that the phase transition is associated with the time reversal symmetry breaking. At the same time, the mean of \tilde{W}_h per hexagon, $\langle \bar{W}_h \rangle = \frac{1}{L^2} \sum_h \langle \tilde{W}_h \rangle$, also increases rapidly around T_c , as shown in Fig. 3(d).

Next, we discuss the data at $x = 0.8$. In contrast to the case of $x = 0$, the specific heat shows two peaks, as shown in Fig. 3(e). The low- T peak is similar to the one in Fig. 3(a), which indicates a phase transition. On the other hand, the high- T peak is broad and does not show the system size dependence. This corresponds to a crossover, and we denote the peak temperature by T^* . Figure 3(f) shows the T dependence of the entropy per site. The entropy is released successively as decreasing T : one third of the entropy, $\frac{1}{3} \ln 2$, is released through the crossover at T^* , and the rest two third $\frac{2}{3} \ln 2$ is released through the phase transition at T_c . The latter is associated with W_t , as indicated by the growth of $\langle \kappa^2 \rangle$ shown in Fig. 3(g). On the other hand, the former comes from \tilde{W}_h ; indeed, as shown in Fig. 3(h), $\langle \bar{W}_h \rangle$ increases around T^* with decreasing T . Therefore, T^* corresponds to the coherent growth of \tilde{W}_h , while T_c corresponds to the time reversal symmetry breaking signaled by the abrupt growth of \tilde{W}_t . Thus, two conserved quantities develop at different T scales at $x = 0.8$, in contrast to the results at $x = 0$, where both grow simultaneously near T_c .

While the phase transition is driven by the last term in Eq. (2), the crossover at T^* is caused by the second term. This is confirmed by considering the second term only, which gives an effective two-level system with the energy splitting $2x$. The specific heat for this system is given by $\tilde{C}_v = \beta^2 x^2 / \cosh^2 \beta x$. The result at $x = 0.8$ is presented by the black curve in Fig. 3(e). This agrees with the MC result near and above T^* .

To determine T_c precisely and to clarify the nature of the phase transition, we performed the finite-size scaling for the order parameter $\langle \kappa^2 \rangle$. Figures 4(a) and 4(b) show the scaling collapses of $\langle \kappa^2 \rangle$ at $x = 0$ and $x = 0.8$, respectively. In both cases, all the data well collapse onto a single universal curve, which indicates that the transitions are of second order. Using the Bayesian scaling analysis for the optimization [20], we obtain the critical temperature and the critical exponents as $T_c = 0.4367(1)$, $1/\nu = 1.027(9)$, and $\eta = 0.243(4)$ for $x = 0$ and $T_c = 0.13906(3)$,

$1/\nu = 1.001(1)$, and $\eta = 0.2545(8)$ for $x = 0.8$. The estimates of ν and η are close to those in the two-dimensional Ising universality class, $\nu = 1$ and $\eta = 1/4$. The results suggest that the phase transitions belong to the two-dimensional Ising universality class, as expected for the Z_2 order parameter κ .

Carrying out the similar analyses while varying x , we obtain the MC phase diagram, as indicated by the red circles in Fig. 2. The x dependence of T_c is similar to that in the MF result, while the values are reduced to roughly half due to thermal fluctuations. Interestingly, the scaling collapse works well for all x , indicating that the phase transition is always of second order in the MC results. This is in clear contrast to the MF result, where both first- and second-order transitions appear with the tricritical point. The results suggest that the tricritical behavior and the first-order transition are the artifact of the MF approximation. In addition to the phase transition, we show the crossover temperature T^* by the orange squares in Fig. 2, which are estimated from the peak T in the specific heat. Near $x = 1$, T^* well agree with $\tilde{T}^* \simeq 0.8336x$ (dashed-dotted line) determined by the peak T of \tilde{C}_v for the two-level system discussed above. With decreasing x from 1, the crossover at T^* merges into the phase transition at T_c , and \tilde{W}_h and \tilde{W}_t grows simultaneously in the smaller x region.

4.3 Comparison to the previous study

Finally, let us compare the present results with those for the original Hamiltonian given in Eq. (1), which were recently obtained by the authors [17]. The present results in the limit of $x \rightarrow 1$ well explain the asymptotic behaviors of T_c and T^* in the limit of $J' \gg J$ for the original model. Moreover, the scaling analysis for much larger system sizes compared to the previous study provides compelling evidence of the second-order phase transition belonging to the two-dimensional Ising universality class in the limit of $J'/J \gg 1$. We note that tricritical behavior was found in the previous study [17], and it looks qualitatively similar to the MF results in the present study. However, this will be just a coincidence, as the tricritical point in the original model is located far from the limit of $J' \gg J$, close to the border between topologically-trivial and nontrivial CSL phases. This is far beyond the effective model used in the present analysis. Moreover, the tricritical behavior in the effective model is an artifact of the MF approximation as discussed above. Further study of more sophisticated effective models including higher-order perturbations will be necessary to clarify the origin of the tricritical behavior. This is left for future study.

5 Conclusion

In summary, we have investigated thermodynamic properties in the isolated dimer limit of the Kitaev-type model on the decorated honeycomb lattice. Using the MF approximation and the unbiased MC simulation, we found that the effective model exhibits a phase transition from paramagnet to the CSL at a finite T . The MC results indicate that the phase transition is always of second order, whereas the MF approximation gives both first- and second-order transitions with a tricritical point. The phase transition is associated with the time reversal symmetry breaking, which is identified by the conserved quantities \tilde{W}_t . In addition to the transition, we found a crossover originating from the coherent growth of the other conserved quantities \tilde{W}_h . With increasing the inter-dimer coupling, the crossover is merged into the phase transition. Moreover, the finite-size scaling analysis indicates that the critical properties of the phase transition are consistent with the two-dimensional Ising universality class. We discussed the results in comparison with those for the original Kitaev-type model.

Acknowledgments. We thank M. Udagawa for fruitful discussion. This work is supported by Grant-in-Aid for Scientific Research No. 15K13533, the Strategic Programs for Innovative Research (SPIRE), MEXT, and the Computational Materials Science Initiative (CMSI), Japan.

References

- [1] Leon Balents. Spin liquids in frustrated magnets. *Nature*, 464(7286):199–208, Mar 2010.
- [2] Vadim Kalmeyer and R. B. Laughlin. Theory of the spin liquid state of the Heisenberg antiferromagnet. *Phys. Rev. B*, 39:11879–11899, Jun 1989.
- [3] Z. Zou, B. Douçot, and B. S. Shastry. Equivalence of fractional quantum hall and resonating-valence-bond states on a square lattice. *Phys. Rev. B*, 39:11424–11427, Jun 1989.
- [4] Kun Yang, L. K. Warman, and S. M. Girvin. Possible spin-liquid states on the triangular and kagomé lattices. *Phys. Rev. Lett.*, 70:2641–2644, Apr 1993.
- [5] Darrell F. Schroeter, Eliot Kapit, Ronny Thomale, and Martin Greiter. Spin hamiltonian for which the chiral spin liquid is the exact ground state. *Phys. Rev. Lett.*, 99:097202, Aug 2007.
- [6] Yin-Chen He, D. N. Sheng, and Yan Chen. Chiral spin liquid in a frustrated anisotropic kagome Heisenberg model. *Phys. Rev. Lett.*, 112:137202, Apr 2014.
- [7] Shou-Shu Gong, Wei Zhu, and D. N. Sheng. Emergent Chiral Spin Liquid: Fractional Quantum Hall Effect in a Kagome Heisenberg Model. *Sci. Rep.*, 4, Sep 2014.
- [8] B. Bauer, L. Cincio, B. P. Keller, M. Dolfi, G. Vidal, S. Trebst, and A. W. W. Ludwig. Chiral spin liquid and emergent anyons in a Kagome lattice Mott insulator. *Nat. Comm.*, 5, Oct 2014.
- [9] Martin Greiter and Ronny Thomale. Non-abelian statistics in a quantum antiferromagnet. *Phys. Rev. Lett.*, 102:207203, May 2009.
- [10] Martin Greiter, Darrell F. Schroeter, and Ronny Thomale. Parent hamiltonian for the non-abelian chiral spin liquid. *Phys. Rev. B*, 89:165125, Apr 2014.
- [11] A Kitaev. Anyons in an exactly solved model and beyond. *Ann. of Phys. (N.Y.)*, 321(1):2–111, Jan 2006.
- [12] Hong Yao and Steven A. Kivelson. Exact chiral spin liquid with non-abelian anyons. *Phys. Rev. Lett.*, 99:247203, Dec 2007.
- [13] Sébastien Dusuel, Kai Phillip Schmidt, Julien Vidal, and Rosa Letizia Zaffino. Perturbative study of the kitaev model with spontaneous time-reversal symmetry breaking. *Phys. Rev. B*, 78:125102, Sep 2008.
- [14] Xiao-Feng Shi, Yan Chen, and J. Q. You. Exotic phase diagram of a topological quantum system. *Phys. Rev. B*, 82:174412, Nov 2010.
- [15] K. S. Tikhonov and M. V. Feigel'man. Quantum spin metal state on a decorated honeycomb lattice. *Phys. Rev. Lett.*, 105:067207, Aug 2010.
- [16] Suk Bum Chung, Hong Yao, Taylor L. Hughes, and Eun-Ah Kim. Topological quantum phase transition in an exactly solvable model of a chiral spin liquid at finite temperature. *Phys. Rev. B*, 81:060403, Feb 2010.
- [17] Joji Nasu and Yukitoshi Motome. Thermodynamics of chiral spin liquids with abelian and non-abelian anyons. *Phys. Rev. Lett.*, 115:087203, Aug 2015.
- [18] Fugao Wang and D. P. Landau. Efficient, multiple-range random walk algorithm to calculate the density of states. *Phys. Rev. Lett.*, 86:2050–2053, Mar 2001.
- [19] Fugao Wang and D. P. Landau. Determining the density of states for classical statistical models: A random walk algorithm to produce a flat histogram. *Phys. Rev. E*, 64:056101, Oct 2001.
- [20] Kenji Harada. Bayesian inference in the scaling analysis of critical phenomena. *Phys. Rev. E*, 84:056704, Nov 2011.